

A temporal record of the past with a spectrum of time constants in the monkey entorhinal cortex

Ian, and Miriam, and Nathan and Zoran and Marc, and Beth (coin flips pending)

Boston University and the University of Washington

Abstract

Episodic memory is believed to be intimately related to our experience of the passage of time. Indeed, neurons in the hippocampus and other brain regions important in episodic memory code for the passage of time at a range of time scales. However, the origin of this temporal signal is thus far unclear. In this study, macaque monkeys viewed a series of complex images for five seconds each. Many neurons in the entorhinal cortex were responsive to image onset. Visually-responsive neurons showed large deviations from baseline firing that peaked shortly after image onset; more than 90% of visually-responsive neurons peaked within 500 ms of stimulus onset. However, different neurons relaxed back to baseline at different rates; several neurons had not returned to baseline even after the entire 5 s had elapsed. Because of the slow relaxation of firing, the ensemble response could be used to decode the time since image onset on the scale of a few seconds. In addition to temporal coding on the scale of seconds, the population also changed gradually across many trials on the scale of minutes. The ensemble carried information about image identity as well as time suggesting that neurons in the entorhinal cortex carry information not only when an event took place but also the identity of that event. Taken together these findings suggest that the monkey entorhinal cortex uses a spectrum of time constants to construct a temporal record of the past for use in episodic memory.

Episodic memory—vivid recollection of an event situated in a specific time and place (Tulving, 1983)—is believed to be an essential function of the medial temporal lobe (MTL), including the hippocampus and entorhinal cortex (EC) (Milner, 1959; Eichenbaum, Yonelinas, & Ranganath, 2007). Building on pioneering work demonstrating a spatial code in the hippocampus and entorhinal cortex (O’Keefe & Dostrovsky, 1971; Fyhn, Molden, Witter, Moser, & Moser, 2004), recent years have shown that hippocampal representations carry information about the time at which past events took place (Pastalkova, Itskov, Amarasingham, & Buzsaki, 2008; MacDonald, Lepage, Eden, & Eichenbaum, 2011) (see (Eichenbaum, 2017) for a recent review), suggesting that the MTL maintains a representation of spatiotemporal context in support of episodic memory. Although a great deal is known about the

temporal coding properties of neurons in the hippocampus, the temporal code in the entorhinal cortex, which provides input to the hippocampus has only just begun to be studied (Naya & Suzuki, 2011; Kraus et al., 2015; Tsao et al., 2018).

Hippocampal *time cells* provide a record of recent events including explicit information about when an event took place. Analogous to hippocampal place cells that fire when the animal is in a circumscribed region of physical space (e.g., Wilson & McNaughton, 1993), hippocampal *time cells* fire during a circumscribed period of time during unfilled delays (MacDonald et al., 2011; Kraus, Robinson, White, Eichenbaum, & Hasselmo, 2013). Across studies, there is a remarkable consistency in the properties of hippocampal time cells (Figure 1). Hippocampal time cells peak at a range of times during the delay interval and code time with decreasing accuracy as the delay unfolds, as manifest by fewer units with peak firing late in the delay and wider time fields later in the delay (e.g., Kraus et al., 2015; Salz et al., 2016; Mau et al., 2018). Hippocampal time cells have been observed in a wide range of tasks, including tasks with and without explicit memory demands during the delay (e.g., Salz et al., 2016), experiments where the animal is fixed in space (MacDonald, Carrow, Place, & Eichenbaum, 2013; Terada, Sakurai, Nakahara, & Fujisawa, 2017), and different stimuli trigger different sequences (Terada et al., 2017; MacDonald et al., 2013). Taken together, time cells provide a record of how far in the past an event—for instance the beginning of a delay period—took place.

Many of the properties of hippocampal time cells have been observed in other brain regions including prefrontal cortex (Bolkan et al., 2017; Tiganj, Kim, Jung, & Howard, 2017; Tiganj, Cromer, Roy, Miller, & Howard, 2018; Jin, Fujii, & Graybiel, 2009) and striatum (Jin et al., 2009; Mello, Soares, & Paton, 2015; Akhlaghpour et al., 2016) suggesting that the hippocampus is part of a widespread network that carries information about what happened when in the past. A recent report from the rat lateral EC adds an important wrinkle to this growing body of literature regarding the representation of time in the brain. Tsao et al. (2018) observed a population of units that changed slowly and reliably enough to decode time within the experiment over a range of time scales. Unlike time cells, which respond a characteristic time since the event that triggers their firing, these units responded immediately to entry into a new environment, and then relaxed slowly (Figure 1c). The relaxation times across individual neurons were very different, ranging from tens of seconds up to thousands of seconds. To distinguish this population from time cells we will refer to neurons that are activated by an event and then relax their firing gradually as *temporal context cells*. Because these temporal context cells code for time, but with very different properties than time cells that have been previously reported, they provide a potentially important clue about the nature of temporal coding in the brain, and thus memory function as well.

This paper will report temporal context cells in monkey EC during performance of a free-viewing task in head-fixed animals (Meister & Buffalo, 2018). We primarily study the firing properties of EC neurons in the five s period after presentation of a visual image. A representation of what happened when should carry information not only about time but also about the identity of events that triggered the firing. Because different images are repeated over the course of the experiment, we will be able to assess this property as well. We argue that units in monkey EC are activated shortly after a visual stimulus and then decay with a variety of rates, properties that are like temporal context cells observed in rat

EC (Tsao et al., 2018) and unlike time cells that have been observed in the hippocampus and other regions (Figure 1). The response of the population will depend on the image presented, suggesting that these temporal context cells also carry information about what happened when. In addition, the population response changes slowly over minutes, suggesting that they could be part of a network for coding a record of history over a range of time scales.

Results

A total of 349 units were recorded from the entorhinal cortex in 2 macaque monkeys during performance of a visual free viewing task. Each trial began with fixation, followed by presentation of a complex visual image that remained on the screen for five seconds of free viewing. Figure 2a shows rasters and PSTH (green dashed line) for three representative units. Unlike canonical hippocampal time cells, which are activated at a variety of points within the delay (e.g., Figure 1a, b), most entorhinal units changed their firing relative to background a short time after the presentation of the visual stimulus. While most of the responsive units increased their firing rate after the stimulus was presented there were some units that decreased their firing rate in response to the presentation of the picture. Although behavior was not controlled during the five second free viewing period, the response of these neurons was consistent across trials (this can be seen by examination of the trial rasters).

Although the image-responsive neurons in EC responded at about the same time post-stimulus, they relaxed back to their baseline firing at different rates. Whereas some neurons relaxed back to baseline quickly (top), some relaxed much more slowly. For instance the unit shown in the bottom of Figure 2a has not returned all the way to baseline even after five seconds.

Quantifying temporal response properties

We modeled each neuron's temporal responsiveness relative to the onset of the visual stimulus based on previous maximum likelihood methods for estimating time cell activity (Tiganj, Shankar, & Howard, 2017). This method is described in detail in the methods (see especially Figure S1c, d). Because the goal of this analysis is to understand the distribution of parameters across units, it is desirable to minimize the noise in the parameter estimates. To this end we used a very conservative criterion to identify temporal context cells (see methods for details). This method identified 129/349 units as temporal context cells. Of those 129 responsive units, 100 units showed an increase in their firing rate in response to stimulus onset while 29 showed a decrease in their firing rate.

Figure 2b summarizes the temporal firing rate properties of these 129 units. Each row of the figure shows the deviation from baseline of each unit over the course of a trial. As can be seen from the figure, almost all of the units reached their maximum deviation from baseline within a few hundred milliseconds of the image presentation. This is in contrast to analogous plots for hippocampal time cells in which different units fire in sequence tiling the delay (e.g., Figure 1a, b). The variability across units in this entorhinal population is not in the time at which the units reach their maximum deviation from baseline, but rather in the time course over which each unit relaxes. This can be seen in the progressive widening of the ridge in Figure 2b from top to bottom.

The maximum likelihood method provides two key parameters that enable us to quantify these properties. The parameter μ approximates the time at which each unit

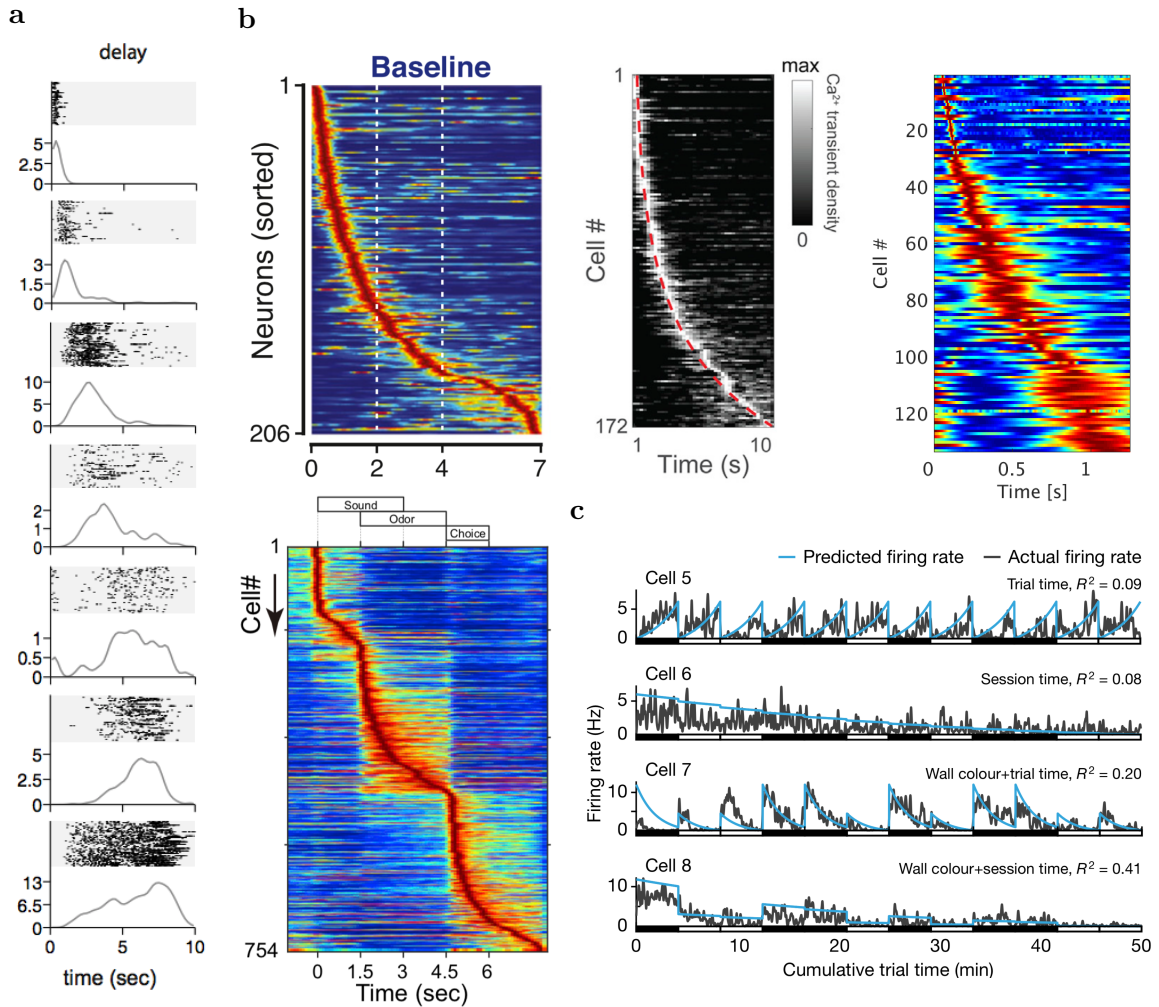


Figure 1. : Coding of Time in the Medial Temporal Lobe. **a**, Rasters of sequentially activated time cells in rat hippocampus. Time cells have receptive fields in time. These fields widen the later a cell fires in the sequence (MacDonald et al., 2011). **b**, Sequentially activated time cells have been observed in rodent and primate hippocampus. Each plot shows the firing rate of a population of units as a function of time during a delay interval. Each row is the firing field of one unit and the units are sorted according to their peak time. Time cells preferentially represent the beginning of the interval, resulting in a characteristic hook when the units are sorted as a function of their peak time. Firing fields later in the delay are also wider. Both of these properties result in lower accuracy in the code for the time of an event with the passage of time (top row: Robinson et al., 2017; Mau et al., 2018; Cruzado et al., 2018, bottom left: Terada et al., 2017). **c**, Recent recordings from rat lateral entorhinal cortex do not show sequentially activated time cells, but rather cells that begin firing shortly following an event and exponentially return to baseline firing rates. (Tsao et al., 2018)

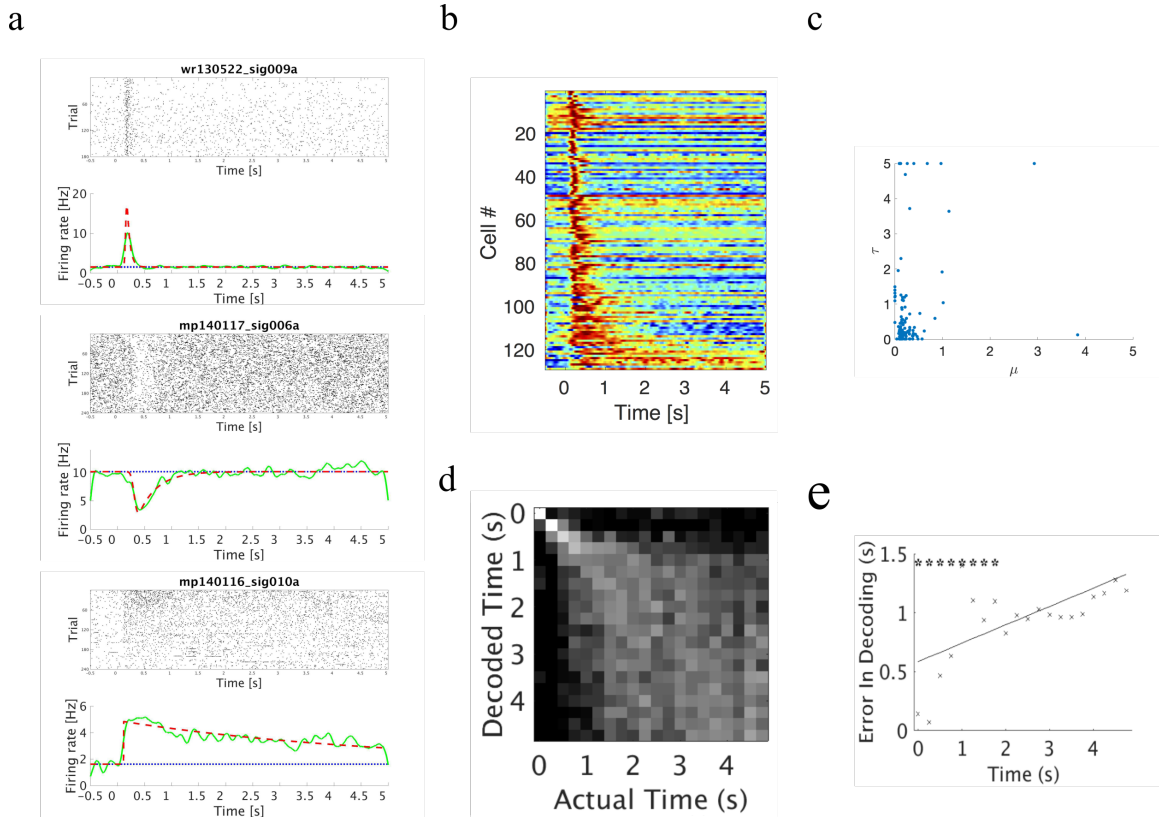


Figure 2. : Temporal context cells in entorhinal cortex respond to the presentation of an image, then relax with a variety of rates, carrying information about time since the image was presented. **a**, Three representative entorhinal units that changed their firing when an image was presented. In each plot, the trial raster is shown relative to the onset of each image. The bottom plot shows the trial averaged firing rate (solid green line) and model estimate of the time course (red dotted line). Many more example units can be found in Supplementary Figure S5. **b**, Trial averaged, normalized firing rates of all entorhinal units that changed their firing when the image was presented, sorted by their time constant. The majority of units responded shortly after image presentation. Many units relaxed back to baseline quickly, but some relaxed more slowly. Across units the population showed a spectrum of decay rates. **c**, Joint distribution across units of parameters μ , an estimate of peak time, and τ , an estimate of relaxation time. Values of μ were clustered around a few hundred ms whereas values of τ spanned the full 5 s of image presentation. **d**, Time since presentation of the image could be decoded from the population of entorhinal units. A linear discriminant analysis (LDA) decoder was trained to decode time and then tested on left-out trials. The x-axis indicates the actual time bin which the LDA attempted to decode. The y-axis indicates the decoded time and the greyscale gives the log of the posterior probability. Perfect decoding would result in a white diagonal. Uniform decoding would result in a grey square. The broad diagonal structure in the empirical results show that decoding is better than chance and decreases in precision with the passage of time. **e**, The average absolute value of decoding error increases with time. Decoding error is the absolute difference between the decoded time and actual time. The decoding error goes up with time, as shown by the fitted regression line (black line). The asterisks mark time bins for which the significance level of the decoding accuracy has been further verified.

reaches its maximum deviation from baseline. Another parameter τ measures how long each unit takes to relax back to its baseline firing rate (see Figure S1d). Figure 2c shows the values of these key parameters for each unit that was categorized as a temporal context cell. The values of μ were clustered at small values. The median value of μ was 160 ms, the interquartile range was 130 ms to 270 ms and 90 % of the units had a value of less than 440 ms. In contrast, τ showed a much wider distribution. For instance, several units had a τ of 5 s, the highest value considered given the five second free viewing period. The mean value of τ was 750 ms with a standard deviation of 1300 ms. The median value of τ was 210 ms, comparable to the value for μ , but the interquartile range was much broader, ranging from 90 ms to 640 ms and 90 % of the units had a value less than 1920 ms.

Noting that the firing fields of hippocampal time cells spread out as the sequence unfolds (Kraus et al., 2013; Howard et al., 2014; Salz et al., 2016), to determine if this property also held for temporal context cells, we examined the relationship between μ , an approximate measure of the time of peak firing of each unit and τ , a measure of unit decay rate. The values of μ and τ measured for temporal context cells in entorhinal cortex were not correlated with one another as measured by a Kendall's τ correlation test, $\tau = .011$, $p > .1$. To assess whether this null effect is reliable, we computed the Bayes factor, a measure of the likelihood of the null hypothesis. This analysis yielded a Bayes factor of $BF_{01} = 8.537$, indicating strong support that unit μ and τ values are uncorrelated. Unlike hippocampal time cells, there is no evidence that temporal context cells that peaked later in the delay showed broader firing fields. In contrast to hippocampal time cells, the overarching conclusion from these analyses is that the firing of entorhinal units deviated from background firing shortly after the presentation of the stimulus and then relaxed exponentially with a variety of time constants independent of peak time.

Decoding time after image presentation from units in monkey entorhinal cortex

It is well-understood that sequentially-activated time cells can be used to decode the time since the beginning of a delay (e.g., Mau et al., 2018, Supplementary information, Figure S2). The accuracy of the temporal decoding can be used to assess the temporal information present in the population of cells. From a theoretical standpoint, we would expect exponentially decaying cells to have temporal information, but to have less information present as time elapses (see simulated data analysis in Supplementary information, Figure S2). A linear discriminant analysis (LDA) was used as the decoder to test this hypothesis. In this analysis the LDA classifier was trained on one subset of the data (the "training data") and tested on another subset of the data (the "testing data"). The training data was the firing rate across units at each of several time bins for a subset of the trials. The testing data was the firing rate across units at each of several time bins for a different subset of the trials. To evaluate the amount of information about time available in the population, the classifier trained to predict the time bin. To the extent the predicted time bin is close to the actual time bin, one can conclude that the population response carried information about time.

Time was decoded better than chance. Figure 2 shows the results of the LDA on the units from monkey entorhinal cortex. Our first question was whether or not the population of temporal context cells contains information about time. The confidence of the decoder,

the posterior distribution, is shown for each actual time bin vs. decoded time bin in Figure 2d). Perfect prediction would correspond to a bright diagonal, random uniform decoding would correspond to a gray square. Qualitatively, the non-uniformity of Figure 2d suggests that elapsed time can be decoded from the entorhinal population. To quantitatively assess this, we found that the posterior distribution from the test data was reliably different from a uniform distribution using a chi-squared goodness of fit test, $\chi^2(X) = 522.17$, $p < .001$.

As an additional test to evaluate whether the population of temporal context cells contains information about time, we computed the mean absolute value of decoding error from the cross-validated LDA. To quantitatively compare this value to chance we compared the true value of decoding error to the distribution of decoding errors across a permuted data set. In each of 1000 permutations we randomly assigned the time bin labels of the training events used to train the classifier. The absolute value of the decoding error for the original data was 1.35 s, which is less (i.e., more accurate) than the mean absolute value of the decoding error for all 1000 permutations (shown in Figure S3, normally distributed with mean 1.66 s, with standard deviation .04 s, $p < .001$ that 1.35 s comes from this distribution). These analyses show that time can be decoded from monkey entorhinal cortex.

The precision of the time estimate decreased as the interval unfolded. Although the population response in entorhinal cortex could be used to reconstruct time, inspection of Figure 2d suggests that the precision of this reconstruction was not constant throughout the interval. Figure 2e shows the average absolute value of the decoding error at each time bin. As can be seen from the figure, this error increased as a function of time. A linear regression of decoding error as a function of time showed a reliable slope (slope of $.18 \pm .04$, intercept $.5 \pm .1$, $p < .001$, $R^2 = .56$, 18 Error degrees of freedom). Thus the temporal information decreases as time elapses.

Time can be decoded out to at least 1.75 seconds. To assess how far into the interval time could be reconstructed, we repeated the LDA analysis excluding progressively more time bins starting from zero. If the LDA can reconstruct time using only bins corresponding to times $\geq t$, then we can (conservatively) conclude that time can be reconstructed at least time t into the interval. To assess this quantitatively, the actual data was compared with permuted data for each repetition of the LDA. The mean of the absolute error across time bins can be used as a metric to compare the performance of the LDA on permutations of the data against its performance on the actual data (see Methods for more details). This permutation testing suggests that time can be decoded up to at least 1.75 seconds from stimulus onset. Thus the population of temporal context cells contains information about time long after the median value of the peak time (160 ms).

The population of EC units changes slowly, on the scale of minutes

The above results show that the population of EC units showed consistent changes in firing on the scale of seconds. Previous work by Tsao et al. (2018) showed units that relaxed over much longer time scales ranging from minutes to hours, such that the population was able to encode temporal information over long time scales. In order to measure whether an analogous slow change also existed in monkey EC, we examined changes in activity across trials. Visual inspection of unit rasters revealed numerous cells that changed their firing

rate over the course of the session (Figure 3a). This pattern was observed for both visually responsive units and units that were not visually responsive. In order to determine which cells showed a slow change in firing, we fit the time series of unit firing during a recording session with a first order autoregressive model. 94/349 units were significantly fit by the model, of which 40/94 were temporal context cells. We then calculated how long the 94 units remained significantly autocorrelated. As seen in Figure 3b the units showed a spectrum of significant autocorrelations. This suggests that individual units in EC systematically change their firing pattern at different rates at longer time scales as well. At the population level, we compared the cosine similarity of simultaneously recorded units during first presentation trials as a function of the recency between trials within the same block. For a given image, the image presented just before would have a recency of 1, the image two before that would have a recency of 2 (Figure 3c, top). Figure 3c, bottom shows a robust effect of recency on population similarity. This impression was confirmed by a linear mixed effects regression, $t(1796) = -12.01, p < 0.0001$. This suggests that the population of monkey EC also shows gradual changes on the scale of minutes.

Firing of EC units was similar for presentations of the same image. In this experiment, each image was presented twice. Although it is not practical to assess image coding using a classifier, it is possible to exploit the repetition of images to determine if entorhinal cortex units contained information about image identity. One possible measure of how the population encoded items is to determine how correlated each unit's spiking activity was during the first and second presentation of images using Kendall's τ , a measure of correlation that is appropriate for non-normal data. If units respond to stimulus identity, spiking activity should show a positive correlation for identical images. The distribution of correlation coefficients across units resulted in a mean that was significantly greater than zero, $t(303) = 6.43, p < 0.0001$, Cohen's $d = 0.3687$, indicating that the population's spiking activity was similar during first and second presentations of items (Fig. S4a). This was confirmed by a Wilcoxon signed rank test, a test that does not assume normality $V = 32931, p < 0.0001$. Further, temporal context cells resulted in a distribution of correlation coefficients with a mean significantly greater than zero, as measured by t-test $t(118) = 5.10, p < 0.0001$, Cohen's $d = 0.4677$ and Wilcoxon signed rank test, $V = 5659, p < 0.0001$. While units that were not identified as temporal context cells also resulted in a distribution with a mean significantly different from zero $t(185) = 3.65, p < 0.01$, Cohen's $d = 0.2673$, $V = 11270, p = 0.0001$ these two distributions were also significantly different from each other by t-test $t(303) = 2.25, p = 0.02$, Cohen's $d = 0.2253$, Wilcoxon rank sum test $V = 9092, p = 0.01$ and permutation analysis 98607/100000. Taken together, this suggests that EC unit spike activity contains information about stimulus identity.

The population of EC units was more similar during image repetition. At the individual unit level, EC responds to stimulus identity. If the response of the entire population contained information about stimulus identity, we would expect, all things equal, that the population vectors corresponding to presentations of the same image would be more similar than the population vectors corresponding to presentations of different images. It is well-known that repeated presentations of a visual image result in less neural firing than initial presentations (Brown & Aggleton, 2001; Meyer & Rust, 2018). To control for the repetition

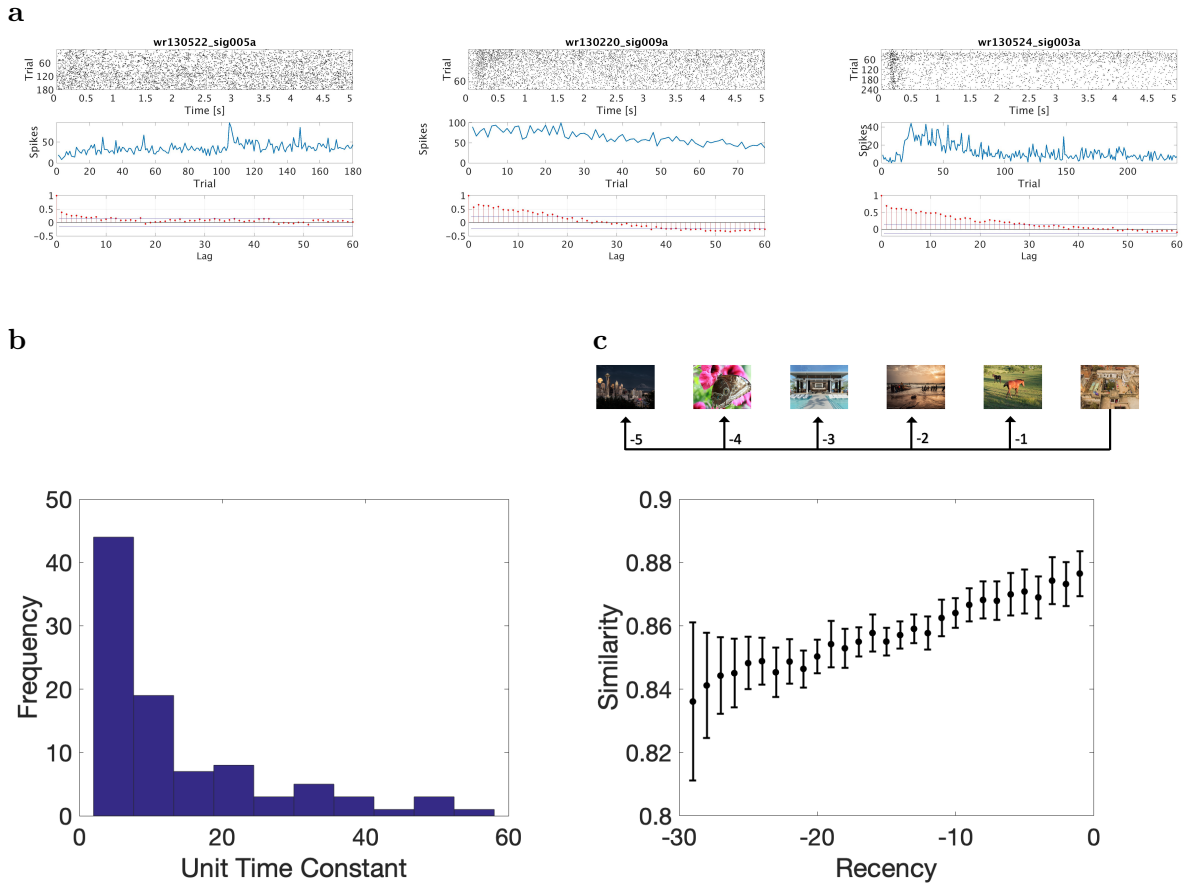


Figure 3. : In addition to coding time on the scale of seconds, the entorhinal population changed gradually over minutes with different units changing at a wide variety of rates. **a**, Many units appeared to change their firing rate systematically over the course of an entire session. In each plot the top panel shows the trial raster aligned to presentation of the image with the first trial at the top. The middle panel shows the number of spikes in the five second interval as a function of trial number. The bottom panel shows the autocorrelation function over trials. We defined the macrotime constant as the largest lag over which the autocorrelation function was above chance. These three units show a variety of macrotime constants from short to long (left to right). The middle and right units were also classified as temporal context cells based on their responsiveness to the image on the scale of seconds. **b**, The distribution of macrotime constants for units that were autocorrelated across trials, as assessed by an AR(1) model. There was a broad spectrum of macrotime constants, with a peak near short times and extending to many dozen trials. Each trial is separated by X seconds, so this corresponds to about Y. **c**, To quantify the drift in the ensemble at the population level, we compared the similarity of the population response as a function of *recency*. Here recency measures the difference in trial number when two population vectors across the five second interval were measured. A recency of 1 compares the population vector from a trial to the preceding trial. The cosine similarity between population vectors changed robustly as a function of recency, meaning that the firing rate of neurons in entorhinal cortex changed slowly across many trials.

effect these analyses compared the similarity between initial presentation of an image and second presentation of the same image to the similarity between second presentations of an image and repetitions of a different first presentation image. Figure S4a shows the results of a population analysis comparing the similarity of the ensemble response to the second presentation of a target image and first presentations of the same image (lag 0) and to first presentations of neighboring images. Images that followed the initial presentation of the target image are associated with positive lags. For instance, lag +1 corresponds to the image that followed the presentation of the target image; lag -1 corresponds to the image that was presented just before the target image. As can be seen from Figure S4b, the similarity to lag 0 was greater than adjacent lags. Statistical comparisons to lags ± 1 each showed a reliable difference. A within block mixed effects regression found that image repetition resulted in a statistically reliable increase in population similarity $t(3758) = 3.59, p < 0.001$, in addition to an increase in similarity for items presented closer together $t(3758) = 8.37, p < 0.0001$. A post-hoc paired t-test comparing population similarity at the block level showed that similarity at lag 0 was reliably larger than at lag +1, $t(63) = 5.11, p < 0.0001$, Cohen's $d = 0.61$, and lag -1, $t(63) = 5.02, p < 0.0001$, Cohen's $d = 0.60$. To evaluate the same hypothesis using a non-parametric method, we performed a permutation analysis by randomly swapping within-session pairs of lag 0 and lag ± 1 and calculating the mean difference between the pairs 100000 times. The observed value exceeded the value of 100000/100000 permuted values for both lags +1 and -1.

Discussion

Episodic memory requires information about both the content of an event as well as its temporal context (Tulving, 1983; Eichenbaum et al., 2007; Eichenbaum, 2017). Many units changed their firing in response to the onset of the visual image. These *temporal context cells* changed at about the same time within a few hundred milliseconds after the image was presented. However, temporal context cells relaxed back to baseline at different rates (see Figure 2). Information about time was implicitly encoded in the slowly relaxing firing rates allowing us to decode the time since image onset over a few seconds (see Figure 2d-e). Notably, the relaxation rate was not constant across units, but rather showed a spectrum of time constants. In addition to temporal information on the scale of seconds, the population also drifted over minutes (see Figure 3). The population vectors following repeated presentations of the same image were more similar to one another than to presentations of different images. This, coupled with several control analyses, enable us to conclude that entorhinal units also carried some information about stimulus identity. Thus, entorhinal units had properties consistent with a temporal record of the past constructed from a spectrum of time constants. Because this record contains information about what happened when, it could be helpful in supporting episodic memory.

Sequentially-activated time cells, such as have been observed in the hippocampus (Pastalkova et al., 2008; MacDonald et al., 2011; Salz et al., 2016), medial entorhinal cortex (Kraus et al., 2015) and many other brain regions (Jin et al., 2009; Mello et al., 2015; Tiganj et al., 2018; Tiganj, Shankar, & Howard, 2017) also show a temporal record of the past. Although the entorhinal temporal context cells provided a temporal record of recent events, they had different firing properties than time cells that have been observed in the hippocampus and other brain regions. Different time cells convey the past time of

occurrence of an event by responding at different temporal lags after the event. Here the temporal context cells all responded at about the same time but relaxed at different rates. This result aligns well with a recent report from rodent LEC (Tsao et al., 2018). In that study LEC neurons responded to a salient event—entering a new environment rather than onset of a visual image—and then changed firing monotonically. Notably, different in that study, as in this one, different units responded at different rates. The similarity of these findings despite the many methodological differences between the two studies—rats moving through a series of open enclosures compared to seated monkeys observing a series of visual images—is striking.

Exponentially-decaying units with a spectrum of time constants is just the Laplace transform of time

This study and a previous rodent study (Tsao et al., 2018) observed entorhinal neurons that code time by gradually change their firing rate with different units changing at different rates. This is in contrast to the temporal coding shown by time cells observed in the hippocampus and other regions. Why would the brain use two such distinct coding schemes to represent the same form of information? It has been proposed (Shankar & Howard, 2012, 2013; Howard et al., 2014) that the brain estimates a temporal record of the past—a function over past time—by first computing the (real) Laplace transform of that function. The Laplace transform of the past with a discrete event would manifest as a set of exponentially-decaying cells with a spectrum of time constants (Howard et al., 2014), very much like the results observed here and in the Tsao et al. (2018) study.

Although it may seem inefficient to estimate the Laplace transform of a function and then invert the transform rather than estimating the function directly, there are several computational advantages to this approach. For instance, in much the same way that the Fourier transform has useful computational properties that make it widely used in signal processing and manipulation, many computations can be more efficiently calculated in the Laplace domain (Howard, Shankar, & Tiganj, 2015). The inverse transform, which takes a set of exponentially-decaying temporal context cells into a set of sequentially-activated time cells, can be implemented using simple center-surround receptive fields in a feed-forward circuit (Shankar & Howard, 2013; Liu, Tiganj, Hasselmo, & Howard, in press). Notably, one can use the same computational framework to compute the Laplace transform of functions other than time, including spatial variables (Howard et al., 2014), accumulated evidence (Howard, Luzardo, & Tiganj, in press) and temporal distance to expected outcomes (Momennejad & Howard, 2018). For instance, border cells observed in rodent and monkey EC (Solstad, Boccaro, Kropff, Moser, & Moser, 2008; Killian, Jutras, & Buffalo, 2012; Hardcastle, Ganguli, & Giocomo, 2015), have properties like one would expect for the Laplace transform of distance to an environmental boundary. In the spatial case, the inverse transform of distance to a boundary would appear as one-dimensional place cells (Gothard, Skaggs, Moore, & McNaughton, 1996; Lever, Burton, Jeewajee, O’Keefe, & Burgess, 2009; Burgess & O’Keefe, 1996). Perhaps temporal context cells and time cells—the Laplace transform and inverse transform of functions of time—are a special case of a more general principle of computational cognitive neuroscience.

Methods

Recording techniques

357 cells were recorded in 2 macaque monkeys over 43 sessions. Of those cells, 349 were located in entorhinal cortex, while 8 were hippocampal cells and were removed from subsequent analyses.

Behavioral task

Analysis of Neural Firing Fields

Spikes were analyzed using a custom maximum likelihood estimation script run in MATLAB 2016a. We calculated model fits across all trials. Fits were compared using a nested maximum likelihood model of each cell's spike train. A likelihood ratio test was performed to calculate the probability that increasing parameters significantly improved a model's fit. This approach is the same as the method used in Salz et al. (2016) and other papers (Tiganj, Kim, et al., 2017; Tiganj et al., 2018) to identify time cells. In the present paper, we considered two models: a constant firing model and, in contrast to the Gaussian model used in the previous papers, we fit spikes to a temporally-modulated convolution of a Gaussian distribution and exponential distribution. The constant model,

$$M_1(t; \theta_1) = a_o \quad (1)$$

consisted of a single parameter a_o that predicted the probability of a spike at time t . The convolution model,

$$M_2(t; \theta_2) = \frac{p}{2} e^{\frac{\lambda}{2}(2\mu + \lambda\sigma^2 - 2t)} \text{erfc}\left(\frac{\mu + \lambda\sigma^2 - t}{\sqrt{2}\sigma}\right) + a_o \quad (2)$$

where erfc is the complementary error function, consisted of five parameters, the constant term a_o , a peak height term p , a decay rate λ from the exponential distribution, and μ and σ from a Gaussian distribution which describes the peak of the distribution and spread of the distribution respectively. μ , σ , and λ are measured in terms of seconds. μ and τ were allowed to take values between 0 and 5 s. σ was allowed to take values between 0 and 1 s. Cell fits were performed over a 5.5 s window, encompassing 5 s of stimulus viewing and .5 s of fixation prior to viewing. Kendall's τ correlation coefficients and Bayes Factors were calculated using JASP statistical software.

Linear Discriminant Analysis

LDA Implementation in Matlab. Time was discretized into bins of 250 ms. For each bin of each trial, the average firing rate was calculated. Training and testing trials were separated by even and odd trials. The number of trials varied for each unit. To mitigate any problems from this, several steps were taken. First, 4 units with less than 30 trials each were entirely excluded from this analysis. Units with less than 200 trials were bootstrapped to 200 trials, while units with more than 200 trials were randomly down-sampled. To avoid errors due to a singular covariance matrix, a small amount of uniform random noise (between 0 and $.25 * 10^{-13}$ spikes/s) was added to the firing rate in each time bin. The averaged firing rate of each time bin for each training trial across all units made

up an element of the training data and the averaged firing rate of each time bin for each testing trial across all units made up an element of the testing data. Linear discriminant analysis was implemented using the Matlab function “classify”. This function takes in the training data, testing data, labels for the training data, and a selection of the method of estimation for the covariance matrix (the option ‘linear’ was used) and returns the resulting classification and a posterior distribution for each element of test data.

LDA Repeated on subduration of time to Further Verify Results. To verify that the temporal information could be decoded across the time interval, the LDA was repeated for successively fewer bins, removing the earliest time bin with each repetition. For each repetition the decoder was tested by training it on permuted data 1000 separate times and then comparing the performance on the permuted vs. un-permuted data by comparing the mean of the absolute error for each permutation. The training data was permuted by randomly shuffling the labels for every training bin. The classifier’s performance was considered better than chance if under 10/1000 permutations performed better than unpermuted data. As quantified with the permutation test, omitting all time bins before 2000 ms (or omitting later than 2000 ms) the decoder did not perform significantly greater than chance level. Thus, entorhinal units can be used to decode time at very least up to at least 1750 ms. This analysis was repeated with larger bins (500 ms) generating a similar result (1500 ms).

Decoding of time from simulated temporal context cells and time cells decreases in precision with the passage of time. In order to illustrate properties of theoretically-motivated models for time coding, we applied the LDA used on the data to two populations of simulated cells. One population was composed of exponentially-decaying temporal context cells with a range of time constants. The other population was chosen to have properties like those observed for hippocampal time cells. One can understand these two populations as encoding the Laplace transform of time since the onset of the stimulus and an approximate inverse of the Laplace transform respectively.

$$\frac{dt(\tau, s)}{d\tau} = \alpha(\tau) [-st(\tau, s) + f(\tau)] \quad (3)$$

To construct this spectrum of time cells, first a spectrum of leaky integrators is constructed (Equation 3). In this equation, τ is time, s is inversely proportional to the time constant of each simulated neuron. t is the activity of each simulated neuron. A spectrum of s are used to get a spectrum of simulated neurons. The input f is a an impulse at time $\tau = 0$. The resulting neurons spike immediately and then decay according to the value of s .

$$T(\tau, s) = \frac{-1^k}{k!} s^{k+1} t^k(\tau, s) \quad (4)$$

$$\overset{*}{\tau} = -\frac{k}{s} \quad (5)$$

Next, Post’s inversion formula (Equation (4)) is used with an approximation of the derivates in order to invert this formula. The result, T , can be thought of as a time shifted ”smeared” approximation of the original input. T is shifted by an amount inversely proportional to s . This amount is the time constant $\overset{*}{\tau}$ (Equation (5)). These differential equations are described in more detail in (Shankar & Howard, 2012).

Exponentially-decaying temporal context cells can be used to decode information about the time at which they were activated. The scale over which each unit contributes maximally to decoding should be on the order of its time constant. The simulated exponentially decaying cells are constructed using Equation (3) with a spectrum of time constants ($\tau^* = -\frac{k}{s}$) ranging from 50 ms to 10000 ms spaced geometrically with a ratio of 1.1 between successive time constants. Note that the figure S2 a does not show all time cells for visual clarity.

This range of time constants means that the smallest time constant is only 1/5 the duration of the bin size, and that the largest time constant is over twice the total duration being decoded. This reduces the possibility of any edge effects. Because there are fewer cells with slow time constants (because of the geometric spacing) and because the firing fields become wider through the interval, decoding accuracy should go down with the passage of time. Figure S2c and e shows results of the same LDA decoder used on the empirical data when applied to this simulated population of temporal context cells.

In addition to the population of exponentially-decaying temporal context cells, we also applied the LDA to a population of model time cells. These time cells were constructed using Equations (3) and (4), with time constants ranging from 50 ms to 10000 ms, spaced geometrically with a ratio of 1.1. Note that the figure S2 b does not show all time cells for visual clarity. This range of time constants means that the smallest time constant is only 1/5 the duration of the bin size, and that the largest time constant is over twice the total duration being decoded. This reduces the possibility of any edge effects altering the analysis. The width of the receptive fields expands with the peak time and because there are fewer neurons with peak times later in the delay, the decoding accuracy of this population of time cells should also go down with the passage of time. Figure S2 d and f shows the results of the LDA applied to this set of simulated time cells. Despite the fact that these two populations have different forms of temporal responsiveness, they both code information about time with the same properties. This is a natural consequence of the fact that the time cell population is just a linear transformation of the temporal context cell population (Shankar & Howard, 2013).

The mean absolute value of error is not precisely linear for several reasons. Edge effects alter the decoding error towards the beginning and end of the duration. The fact that the decoder is a linear decoder while the underlying encoding (exponentially decaying cells and time cells) is not linearly also partially accounts for the nonlinear change in decoding error.

Autocorrelation

For each unit, we calculated if the time series of spike counts during image presentation was significantly fit by an AR(1) model as measured by Akaike information criterion, using the “ar” function in R. Only units that averaged a firing rate of at least 2 Hz during image presentation and were recorded for at least 60 trials were considered. Once units were identified using this method, we then measured at what lags those units showed a significant autocorrelation using the “autocorr” function in Matlab. We considered the length of a unit’s autocorrelation to be the lag just prior to the smallest lag at which the unit was no longer significantly autocorrelated.

Population Similarity

For each item we created two population vectors, one during first presentation and one during second presentation. Each vector was created from the mean firing activity of all the available units, such that vector length was equal to the number of available units. Mean firing rates were normalized by each unit's maximum average firing rate so that firing rates ranged from 0 to 1. Only blocks where all images were presented twice were considered. In order to control for different block lengths between sessions, only the first 30 images presented in each block were used. Lag was the distance between the first presentation of an image and another image, and ranged from -29 to 29. Recency was the distance between every pair of first presentation images in the same block and ranged from 1 to 29. Similarity was measured by measuring the cosine similarity of the two population vectors. The linear mixed effects model was calculated using R, with the packages “plyr”, “lme4”, and “lmerTest”. Spike correlations were calculated by determining the number of spikes in each trial. Spikes were then compared across first and second presentations of images.

References

- Akhlaghpour, H., Wiskerke, J., Choi, J. Y., Taliaferro, J. P., Au, J., & Witten, I. (2016). Dissociated sequential activity and stimulus encoding in the dorsomedial striatum during spatial working memory. *eLife*, 5, e19507.
- Bates, D., Mächler, M., Bolker, B., & Walker, S. (2014). Fitting linear mixed-effects models using lme4. *arXiv preprint arXiv:1406.5823*.
- Bolkan, S. S., Stujenske, J. M., Parnaudeau, S., Spellman, T. J., Rauffenbart, C., Abbas, A. I., ... Kellendonk, C. (2017). Thalamic projections sustain prefrontal activity during working memory maintenance. *Nature Neuroscience*, 20(7), 987–996. Retrieved from <http://dx.doi.org/10.1038/nn.4568>
- Brown, M. W., & Aggleton, J. P. (2001). Recognition memory: what are the roles of the perirhinal cortex and hippocampus? *Nature reviews. Neuroscience*, 2(1), 51-61.
- Burgess, N., & O'Keefe, J. (1996). Neuronal computations underlying the firing of place cells and their role in navigation. *Hippocampus*, 6(6), 749-62.
- Cruzado, N. A., Tiganj, Z., Brincat, S. L., Miller, E. K., & Howard, M. W. (2018). Compressed temporal representation during visual paired associate task in monkey prefrontal cortex and hippocampus. In *Program no. 243.03 2018 neuroscience meeting planner*. San Diego, CA: Society for Neuroscience.
- Eichenbaum, H. (2017). On the integration of space, time, and memory. *Neuron*, 95(5), 1007-1018. doi: 10.1016/j.neuron.2017.06.036
- Eichenbaum, H., Yonelinas, A., & Ranganath, C. (2007). The medial temporal lobe and recognition memory. *Annual Review of Neuroscience*, 30, 123-152.
- Fyhn, M., Molden, S., Witter, M. P., Moser, E. I., & Moser, M. B. (2004). Spatial representation in the entorhinal cortex. *Science*, 305(5688), 1258-64.
- Gothard, K. M., Skaggs, W. E., Moore, K. M., & McNaughton, B. L. (1996). Binding of hippocampal CA1 neural activity to multiple reference frames in a landmark-based navigation task. *Journal of Neuroscience*, 16(2), 823-35.
- Hardcastle, K., Ganguli, S., & Giocomo, L. M. (2015). Environmental boundaries as an error correction mechanism for grid cells. *Neuron*, 86(3), 827-839.
- Howard, M. W., Luzardo, A., & Tiganj, Z. (in press). Evidence accumulation in a laplace decision space. *Computational Brain and Behavior*.

- Howard, M. W., MacDonald, C. J., Tiganj, Z., Shankar, K. H., Du, Q., Hasselmo, M. E., & Eichenbaum, H. (2014). A unified mathematical framework for coding time, space, and sequences in the hippocampal region. *Journal of Neuroscience*, 34(13), 4692-707. doi: 10.1523/JNEUROSCI.5808-12.2014
- Howard, M. W., Shankar, K. H., & Tiganj, Z. (2015). Efficient neural computation in the Laplace domain. In *Cognitive computation: Integrating neural and symbolic computation*.
- Jin, D. Z., Fujii, N., & Graybiel, A. M. (2009). Neural representation of time in cortico-basal ganglia circuits. *Proceedings of the National Academy of Sciences*, 106(45), 19156–19161.
- Killian, N. J., Jutras, M. J., & Buffalo, E. A. (2012). A map of visual space in the primate entorhinal cortex. *Nature*, 491(7426), 761-4. doi: 10.1038/nature11587
- Kraus, B. J., Brandon, M. P., Robinson, R. J., Connerney, M. A., Hasselmo, M. E., & Eichenbaum, H. (2015). During running in place, grid cells integrate elapsed time and distance run. *Neuron*, 88(3), 578–589.
- Kraus, B. J., Robinson, R. J., 2nd, White, J. A., Eichenbaum, H., & Hasselmo, M. E. (2013). Hippocampal "time cells": time versus path integration. *Neuron*, 78(6), 1090-101. doi: 10.1016/j.neuron.2013.04.015
- Kuznetsova, A., Brockhoff, P. B., & Christensen, R. H. B. (2017). lmertest package: tests in linear mixed effects models. *Journal of Statistical Software*, 82(13).
- Lever, C., Burton, S., Jeewajee, A., O'Keefe, J., & Burgess, N. (2009). Boundary vector cells in the subiculum of the hippocampal formation. *Journal of Neuroscience*, 29(31), 9771-7.
- Liu, Y., Tiganj, Z., Hasselmo, M. E., & Howard, M. W. (in press). A neural microcircuit model for a scalable scale-invariant representation of time. *Hippocampus*.
- MacDonald, C. J., Carrow, S., Place, R., & Eichenbaum, H. (2013). Distinct hippocampal time cell sequences represent odor memories immobilized rats. *Journal of Neuroscience*, 33(36), 14607–14616.
- MacDonald, C. J., Lepage, K. Q., Eden, U. T., & Eichenbaum, H. (2011). Hippocampal "time cells" bridge the gap in memory for discontiguous events. *Neuron*, 71(4), 737-749.
- Mau, W., Sullivan, D. W., Kinsky, N. R., Hasselmo, M. E., Howard, M. W., & Eichenbaum, H. (2018). The same hippocampal CA1 population simultaneously codes temporal information over multiple timescales. *Current Biology*, 28, 1499-1508.
- Meister, M. L., & Buffalo, E. A. (2018). Neurons in primate entorhinal cortex represent gaze position in multiple spatial reference frames. *Journal of Neuroscience*, 38(10), 2430–2441.
- Mello, G. B., Soares, S., & Paton, J. J. (2015). A scalable population code for time in the striatum. *Current Biology*, 25(9), 1113–1122.
- Meyer, T., & Rust, N. C. (2018). Single-exposure visual memory judgments are reflected in inferotemporal cortex. *eLife*, 7. doi: 10.7554/eLife.32259
- Milner, B. (1959). The memory defect in bilateral hippocampal lesions. *Psychiatric research reports*, 11, 43.
- Momennejad, I., & Howard, M. W. (2018). Predicting the future with multi-scale successor representations. *bioRxiv*, 449470.
- Naya, Y., & Suzuki, W. (2011). Integrating what and when across the primate medial temporal lobe. *Science*, 333(6043), 773-776.
- O'Keefe, J., & Dostrovsky, J. (1971). The hippocampus as a spatial map. preliminary evidence from unit activity in the freely-moving rat. *Brain Research*, 34(1), 171-175.
- Pastalkova, E., Itskov, V., Amarasingham, A., & Buzsaki, G. (2008). Internally generated cell assembly sequences in the rat hippocampus. *Science*, 321(5894), 1322-7.
- Robinson, N. T., Priestley, J. B., Rueckemann, J. W., Garcia, A. D., Smeglin, V. A., Marino, F. A., & Eichenbaum, H. (2017). Medial entorhinal cortex selectively supports temporal coding by hippocampal neurons. *Neuron*, 94(3), 677–688.
- Salz, D. M., Tiganj, Z., Khasnabish, S., Kohley, A., Sheehan, D., Howard, M. W., & Eichenbaum, H. (2016). Time cells in hippocampal area CA3. *Journal of Neuroscience*, 36, 7476-7484.

- Shankar, K. H., & Howard, M. W. (2012). A scale-invariant internal representation of time. *Neural Computation*, 24(1), 134-193.
- Shankar, K. H., & Howard, M. W. (2013). Optimally fuzzy temporal memory. *Journal of Machine Learning Research*, 14, 3753-3780.
- Solstad, T., Boccaro, C. N., Kropff, E., Moser, M. B., & Moser, E. I. (2008). Representation of geometric borders in the entorhinal cortex. *Science*, 322(5909), 1865-8.
- Terada, S., Sakurai, Y., Nakahara, H., & Fujisawa, S. (2017). Temporal and rate coding for discrete event sequences in the hippocampus. *Neuron*, 94, 1-15.
- Tiganj, Z., Cromer, J. A., Roy, J. E., Miller, E. K., & Howard, M. W. (2018). Compressed timeline of recent experience in monkey iPFC. *Journal of Cognitive Neuroscience*, 30, 935-950.
- Tiganj, Z., Kim, J., Jung, M. W., & Howard, M. W. (2017). Sequential firing codes for time in rodent mPFC. *Cerebral Cortex*, 27, 5663-5671.
- Tiganj, Z., Shankar, K. H., & Howard, M. W. (2017). Scale invariant value computation for reinforcement learning in continuous time. In *AAAI 2017 spring symposium series - science of intelligence: Computational principles of natural and artificial intelligence*.
- Tsao, A., Sugar, J., Lu, L., Wang, C., Knierim, J. J., Moser, M.-B., & Moser, E. I. (2018). Integrating time from experience in the lateral entorhinal cortex. *Nature*, 561, 57-62. Retrieved from <https://doi.org/10.1038/s41586-018-0459-6> doi: 10.1038/s41586-018-0459-6
- Tulving, E. (1983). *Elements of episodic memory*. New York: Oxford.
- Wickham, H., et al. (2011). The split-apply-combine strategy for data analysis. *Journal of Statistical Software*, 40(1), 1-29.
- Wilson, M. A., & McNaughton, B. L. (1993). Dynamics of the hippocampal ensemble code for space. *Science*, 261, 1055-8.

Supplementary Information

Modeling properties of temporal responsive units

Increases in μ shift the curve to the right and increases in τ lengthen the curve's decay rate (Figure S1)d. An additional model parameter σ measures the deviation from exponentially-decaying firing.

Properties of σ , μ and τ for idealized time cells and Temporal Context Cells. As shown in Figure S1, populations of theoretical time cells and temporal context cells result in different distributions of parameters. Time cell peaks (μ) span the entirety of a time interval, and cell peaks over-represent the beginning of a delay. Time cell receptive fields widen (σ) and become increasingly skewed (τ) the later in the delay they peak. As a result, these parameters are all positively correlated with one another for a population of time cells. Temporal context cells peak (μ) at the beginning of a time interval. The decay rate (τ) of temporal context cells should span the interval, with more smaller values of τ than larger values. In temporal context cells, σ measures the deviation from a purely exponential curve and should be very small.

It is straightforward to compute the relationships between μ and τ across units for two forms of temporal coding. For a population of temporal context cells coding for the Laplace transform of time since presentation of a stimulus, the responsive of unit i should be given by

$$F(t > 0) = A_i + B_i e^{-t/\tau_i} \quad (\text{S1})$$

where A_i and B_i are parameters describing the baseline firing rate and amplitude of modulation of unit i , τ_i is the time constant of unit i . The set of units described by this expression provide the Laplace transform of t the time at which the stimulus was experienced.

If a population of units were described by Eq. S1, we would expect to see a large degree of variability in the estimates of σ . μ should describe the latency between when the stimulus is presented and it conveys information to the neurons. We would expect μ to be the same across units that encode Eq. S1.

TODO: Analogous walk through the equation and each of the parameters.

$$A_i + B_i t^k e^{-s_i t} \quad (\text{S2})$$

Empirical results for model parameters. Results for μ and τ are discussed in detail in the main text. The values of σ were small and tightly clustered.

Temporal decoding from ideal sequentially-activated time cells and exponentially-decaying units

This technique is demonstrated on simulated exponentially decaying cells and simulated time cells in Figure S2. The decoding error appears to behave similarly for both ideal time cells and exponentially decaying cells.

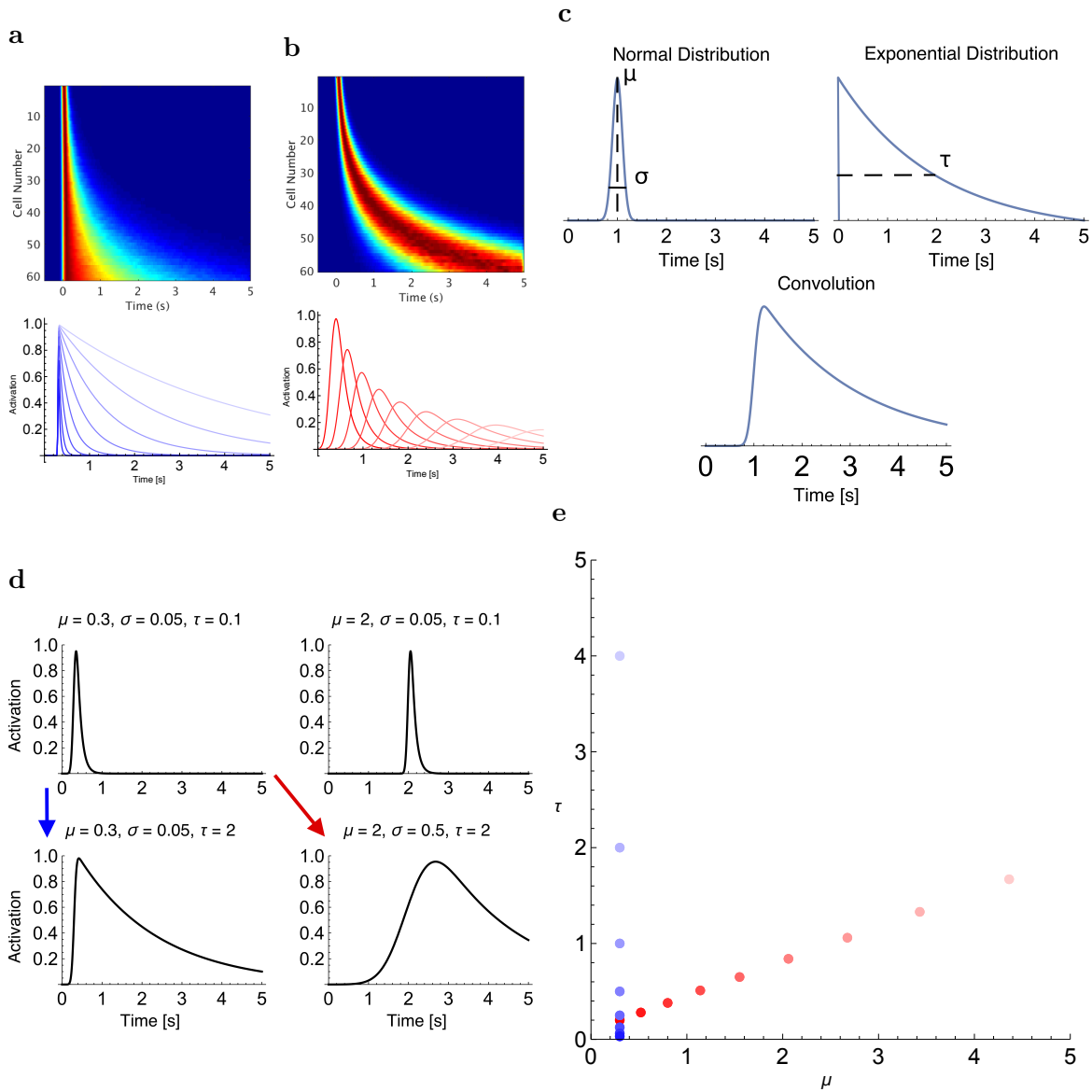


Figure S1. : Two Ways of Encoding the Recent Past. **a**, Top, heatplot of ideal exponentially decaying cells. Bottom, tuning curves of exponentially decaying cells. Cells all peak at the beginning of a time interval, but decay at different rates, as indicated by line shade. **b**, Top, heatplot of ideal sequentially activated time cells. Bottom, tuning curves of time cells. Cell peaks span a given time interval, as indicated by line shade, and widen their receptive field the later in a time interval they peak. **c**, The convolution model (bottom) is formed by the combination of a Gaussian distribution, with parameters μ and σ and an exponential distribution, with parameter τ (top). **d**, In the convolution model, an increase in μ shifts the distribution to the right, an increase in σ widens the entire distribution, and an increase in τ lengthens its decay rate. The blue and red arrows correspond to the parameter changes expected of exponentially decaying and sequentially activated time cells respectively. **e**, Values of μ and τ of the cells plotted in the bottom of **a** and **b**. A population of exponentially decaying cells all have small μ values but show a variety of τ values. Time cells show values of μ that span a time span, with τ values that increase with μ .

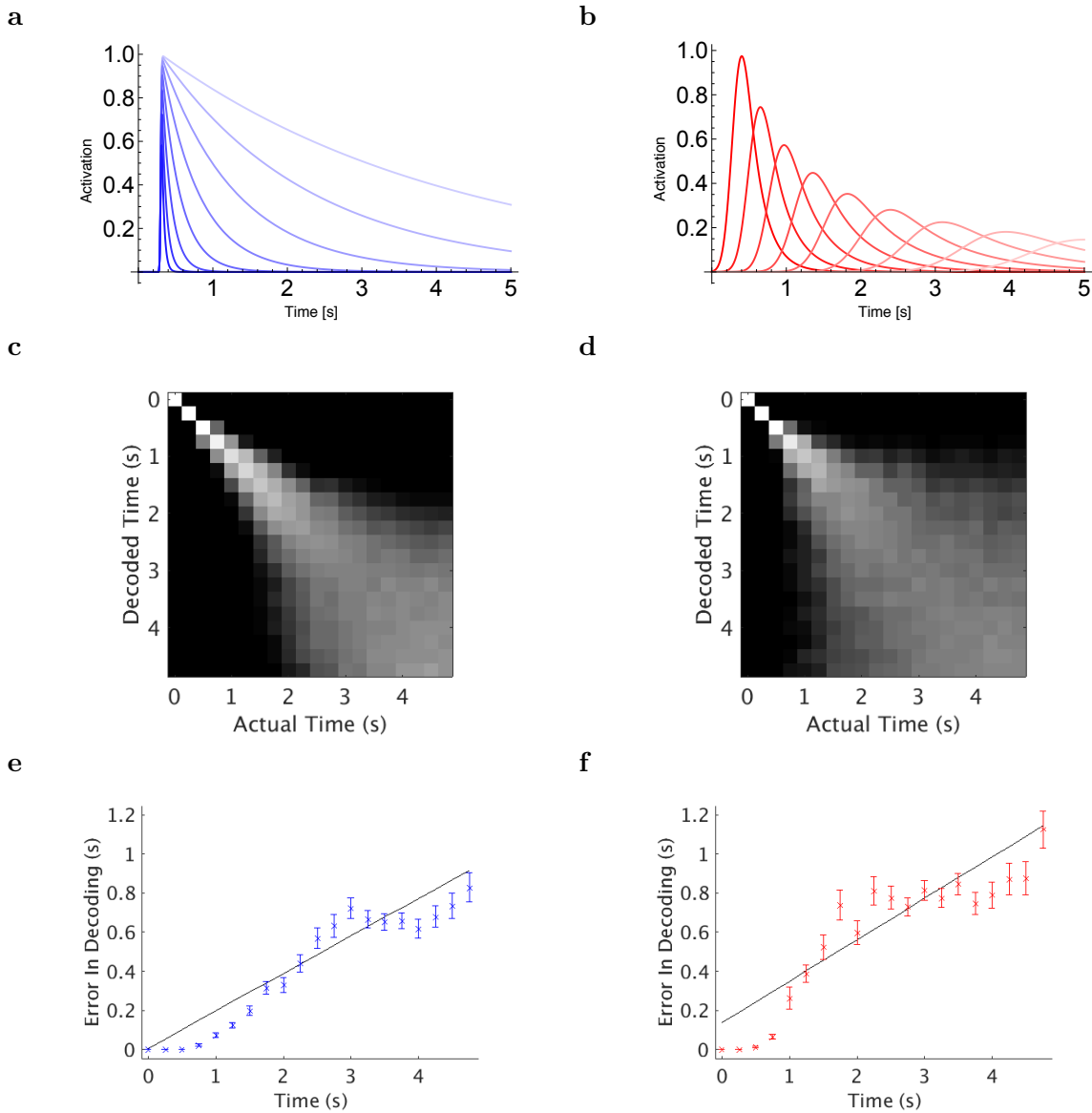


Figure S2. : **Time can be decoded from both time cells and exponentially decaying cells with decreasing accuracy as time unfolds.** Simulated noisy time cells and exponentially decaying cells. Time is binned in 250ms bins. A linear decoder is trained on odd trials and tested on even trials. **a** An illustration of a small collection of exponentially decaying cells. The actual simulated data set used 30 cells with time constants ranging from 50 ms to 10s. **b** An illustration of a collection of ideal time cells. The actual simulated data set used 30 cells with time constants ranging from 50ms to 10s. **c, d** Log of the posterior probabilities. The posterior probabilities of the classify function are averaged across trials for each time bin. Perfect decoding would look like a white diagonal. In order to show the distinction between small values, the log of the averaged posterior probabilities plus a small threshold is shown here. The posterior distribution of the classifier shows an increasing spread in the model's estimation of decoded time. **e, f** Averaged absolute value of decoding error. The decoding error goes up with time, as shown by the fitted regression line (black line).

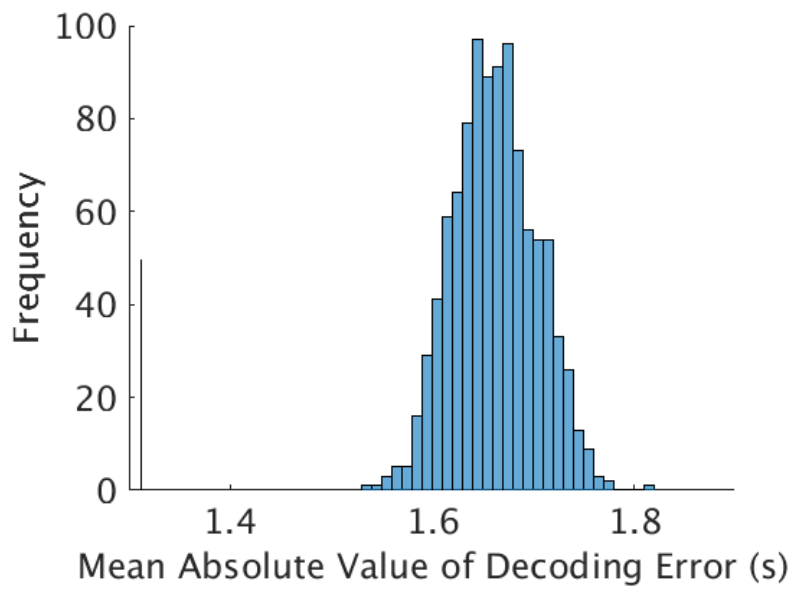


Figure S3. : Data with permuted labels contains less information than the original data.. The histogram shows the distribution of mean absolute value of decoding error for the permuted data. The mean absolute value of decoding error for the original data is marked with the line. The original data's decoding error is clearly different from that of the permuted data. This indicates the decoding is significantly better than chance.

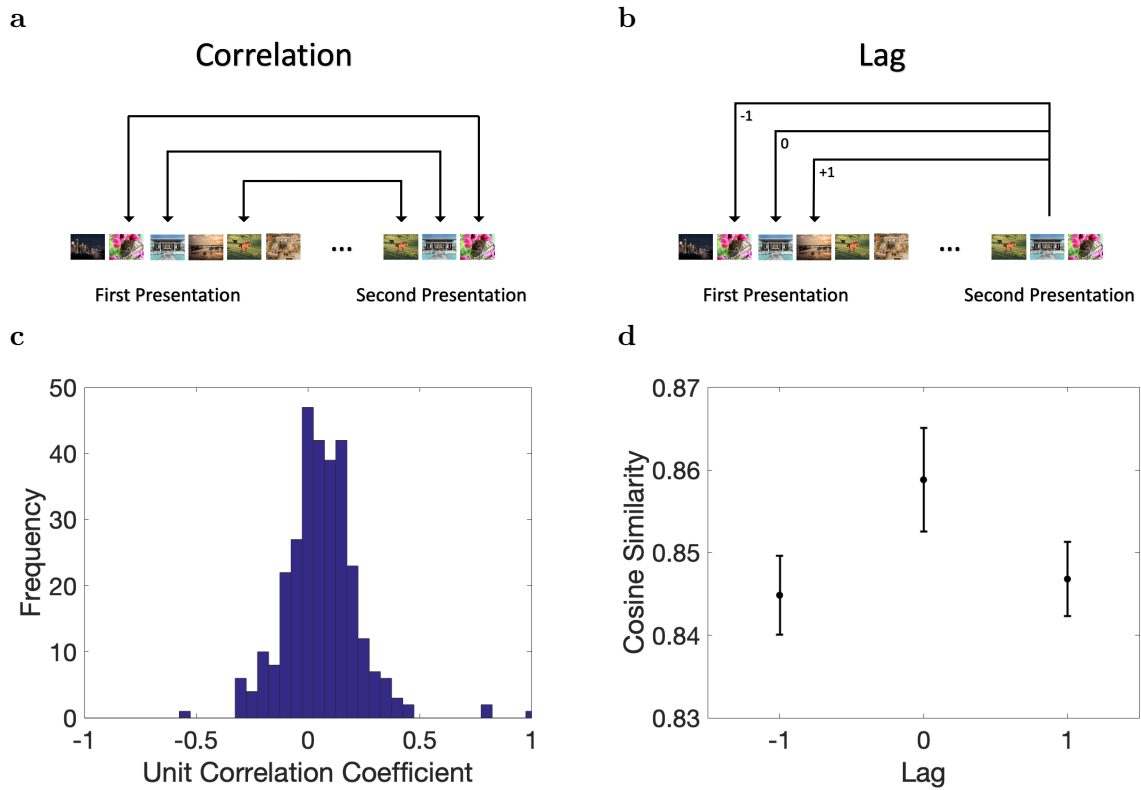


Figure S4. : The Entorhinal Ensemble Carries Information About Stimulus Identity. **a**, At the unit level, we measured how correlated spiking activity was in response to the same image, as measured by Kendall's τ . **b**, In lag analyses the population of cells during the second presentation of an image is compared to the population of cells during the first presentation of all images. **c**, Across the population, unit spiking activity in response to image repetition was positively correlated. **d**, There is a significant spike in image similarity at lag zero (image repetition) compared to lag +1 and lag -1 (adjacent images).

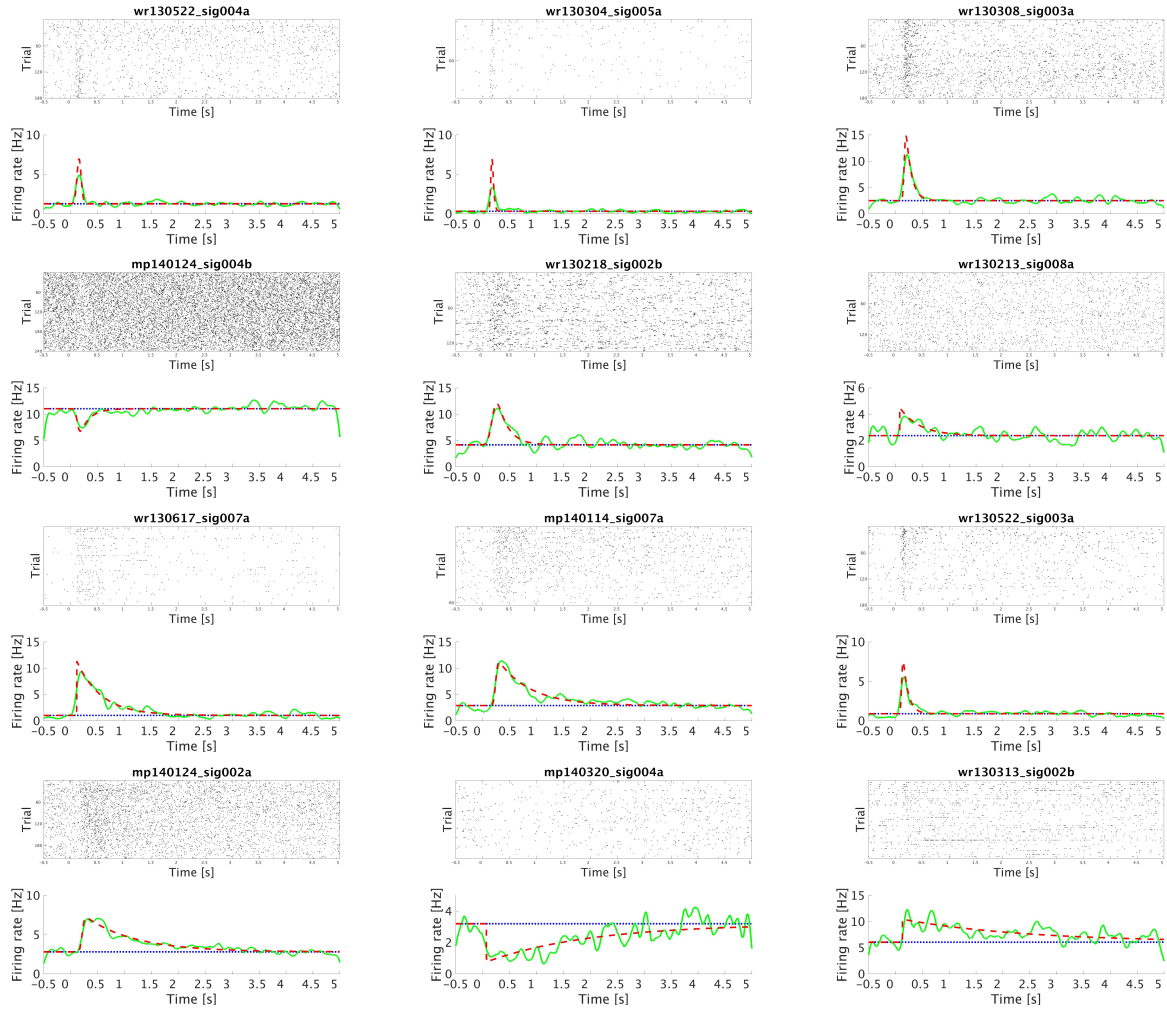


Figure S5. : Additional examples of temporal context cells. Format is as in Figure 2a. Units are ordered by their estimated relaxation rate (τ).